Journal of Chemical Health Risks

www.jchr.org

JCHR (2025) 15(2), 701-713 | ISSN:2251-6727

Design and Optimization of Green-Synthesized Silver Nanoparticles Functionalized with Folic Acid and Curcumin-HC for Targeted Breast Cancer Treatment

[1]Bipul Nath*, [1]Runa Chakravorty[1], [1]Manas Jyoti Kapil[2], [1]Neelakshi Sharma[3], [2]Subhashis Debanath[4]

[1]Department of Pharmacy, Royal School of Pharmacy, The Assam Royal Global University, Betkuchi, Guwahati, Assam-781035, INDIA.

[2]Department of Pharmacy, Bharat Pharmaceutical Technology, Amtali, Agartala, West Tripura, Tripura- 799130, INDIA.

(Received: 16 January 2025 Revised: 20 Feburary 2025 Accepted: 31 March 2025)

KEYWORDS

Green-synthesized silver nanoparticles, Folate receptor, Curcumin, Enhanced bioavailability, Targeted drug delivery, Breast cancer, Apoptosis

ABSTRACT:

Introduction: Breast cancer remains a leading global health concern, with rising incidence and mortality rates. Conventional treatments face challenges like systemic toxicity and drug resistance, necessitating novel therapeutic strategies. This study explores a green-synthesized, folic acid-functionalized curcumin-silver nanoparticle system for targeted breast cancer therapy, enhancing drug bioavailability, therapeutic efficacy, and minimizing adverse effects.

Objectives: Developing green-synthesized, folic acid-functionalized curcumin-silver nanoparticles for targeted breast cancer therapy, enhancing bioavailability, efficacy, and reducing toxicity.

Methods: Houttuynia cordata roots were extracted using hydroalcoholic maceration. Green-synthesized AgNPs were prepared by mixing $AgNO_3$ with H. cordata extract. PEGylation was achieved via ligand exchange, followed by curcumin conjugation. Folic acid functionalization was conducted using EDC/NHS activation. Nanoparticles were characterized using UV-Vis, FT-IR, TEM, SEM, and zeta potential analysis. Drug loading, entrapment efficiency, and in-vitro curcumin release were evaluated. Cytotoxicity studies on MCF-7 cells included MTT assays and AO-EtBr dual staining for apoptosis detection.

Results: The study synthesized folic acid- and curcumin-functionalized silver nanoparticles (FA-Cur-Hc-AgNPs) using Houttuynia cordata extract. Characterization confirmed stability, efficient drug loading (72–94.12%), and pH-responsive curcumin release (73.32% at pH 5.5). FA-Cur-Hc-AgNPs exhibited cytotoxicity against MCF-7 cells, inducing apoptosis. These findings highlight their potential as a targeted nanotherapeutic for breast cancer treatment.

Conclusions: FA-Cur-Hc-AgNPs were successfully synthesized and functionalized, demonstrating stability, targeted delivery, and pH-responsive drug release. They exhibited potent cytotoxicity against MCF-7 cells, inducing apoptosis. These findings highlight their potential as a promising nanotherapeutic for breast cancer, suggesting further in-vivo studies.

1. Introduction

Cancer remains a significant global health burden, with over 20 million new cases and approximately 10 million deaths recorded annually. The incidence of cancer is steadily rising, with projections indicating a surge to nearly 28 million cases by 2040. Among various malignancies, breast cancer is the most frequently diagnosed, accounting for an estimated 2.3 million new cases in 2020, according to the World Health Organization (WHO). Primarily affecting adolescent and middle-aged women, the rising prevalence and mortality rates of breast cancer emphasize the urgent need for effective therapeutic interventions [1-3].

Journal of Chemical Health Risks

www.jchr.org

JCHR (2025) 15(2), 701-713 | ISSN:2251-6727

Several risk factors contribute to the increasing incidence of breast cancer, including early onset of menstruation, late menopause, obesity, hormone replacement therapy, sedentary lifestyles, and reduced breastfeeding. Conventional treatment modalities such as chemotherapy, radiotherapy, and surgical resection remain the mainstay of breast cancer management. However, these approaches are often associated with significant challenges, including systemic toxicity, non-specific drug distribution, and drug resistance. Consequently, there is an imperative need for novel therapeutic strategies to enhance treatment efficacy while minimizing adverse effects [4, 5].

Nanotechnology has emerged as a transformative approach in cancer therapy, leading to the development of cancer nanomedicine. Silver nanoparticles (AgNPs) have gained particular interest due to their unique physicochemical and biological properties, including anticancer, antimicrobial, and antioxidant activities [6]. The biosynthesis of AgNPs, particularly through green synthesis methods, is gaining momentum as an eco-friendly and sustainable alternative to conventional chemical and physical synthesis techniques. Green synthesis leverages biological entities such as plants, fungi, and bacteria to produce nanoparticles with improved biocompatibility and reduced toxicity [7, 8].

Houttuynia cordata (H. cordata), a well-documented medicinal plant, has demonstrated significant pharmacological properties, including antibacterial, antiviral, antioxidant, anti-inflammatory, and anticancer effects [9,10]. Its bioactive compounds serve as natural reducing and stabilizing agents in the green synthesis of AgNPs, ensuring stability and enhanced therapeutic potential. The utilization of H. cordata-mediated AgNPs presents a promising avenue for cancer treatment by offering a cost-effective and environmentally sustainable method for nanoparticle synthesis [11-14].

Curcumin, a polyphenolic compound derived from Curcuma longa, has garnered extensive scientific attention due to its potent anti-inflammatory, antioxidant, antibacterial, antifungal, and anticancer properties [14,15]. However, its clinical application is hindered by poor aqueous solubility, low bioavailability, and rapid systemic metabolism. To overcome these limitations, nanotechnology-based drug delivery systems have been explored, wherein curcumin is encapsulated in nanoparticle-polymer conjugates to enhance its solubility, stability, and targeted delivery while preserving its therapeutic efficacy [16-20].

Folate receptor (FR)-targeted drug delivery systems have emerged as a promising approach for cancer therapy. The folate receptor, specifically the FRα isoform, is overexpressed in various cancerous tissues, including breast, ovarian, lung, and colon tumors, while being minimally expressed in normal cells. This differential expression makes folic acid an ideal ligand for targeted drug delivery, ensuring site-specific therapeutic action with reduced off-target effects [20-21].

In this study, a novel therapeutic strategy is proposed, involving the green synthesis of AgNPs using H. cordata aqueous extract, followed by conjugation with curcumin (Cum). The resulting curcumin-silver nanoparticle-polymer conjugate (Cum–PEG–HcAgNPs) is further functionalized with folic acid to facilitate targeted delivery to folate receptor-overexpressing breast cancer cells. This innovative approach aims to improve drug bioavailability, enhance therapeutic efficacy, and reduce systemic toxicity, presenting a promising direction for future breast cancer treatment advancements.

2. Objectives

The study aimed to develop an eco-friendly approach for synthesizing silver nanoparticles using Houttuynia cordata extract as a natural reducing and stabilizing agent. The synthesized nanoparticles were conjugated with curcumin to enhance its stability, solubility, and bioavailability, addressing its poor aqueous solubility. Further functionalization with folic acid was employed to facilitate targeted drug delivery to folate receptor-overexpressing breast cancer cells, increasing cellular uptake via receptor-mediated endocytosis. The research focused on optimizing nanoparticle stability through polymer conjugation and achieving controlled, sustained drug release to minimize non-specific drug distribution and systemic toxicity. By enhancing therapeutic efficacy while reducing adverse effects, the study sought to improve the overall efficiency of nanomedicine-based cancer treatments. Additionally, the potential of *Houttuynia cordata* in nanomedicine was explored for its bioactive properties. The findings contribute to advancing targeted nanotherapeutics for

Journal of Chemical Health Risks

www.jchr.org

JCHR (2025) 15(2), 701-713 | ISSN:2251-6727

breast cancer treatment, offering a promising strategy for improving drug delivery and therapeutics.

3. Materials and Methods

Silver nitrate, folic acid, curcumin, N-hydroxysuccinimide, sodium dihydrogen phosphate, ethyl dimethylaminopropyl carbodiimide, NaOH, PEG 2000, and potassium dihydrogen phosphate were sourced from Sigma-Aldrich. Milli-Q water, deoxygenated with nitrogen, was used throughout the synthesis and formulation of green silver nanoparticles. All chemicals employed in this study were of analytical grade, guaranteeing high purity and reliability for precise experimental outcomes.

Plant Collection, Authentication, and Extraction

The whole plant material of Houttuynia cordata (Thunb.) was sourced from NEDFi, Assam, India. For extraction, the roots of H. cordata were shade-dried and ground into a coarse powder using a grinder. An accurately weighed 400 g sample of the powdered root was subjected to extraction using the cold maceration method with a hydroalcoholic solvent (ethanol: water, 70:30) at room temperature for three consecutive days [22]. The extract was then filtered through filter paper and concentrated under reduced pressure using a rotary evaporator (IKA, VC10 Lite, Germany) at 45 ± 2°C. The resulting residue was lyophilized to obtain a dry extract, which was stored in a glass container for further analysis. The extraction yield was determined to be 10.5% w/w.

Green Synthesis of Hc-AgNPs Using Aqueous H. cordata Extract

A 1 M stock solution of silver nitrate ($AgNO_3$) was prepared. The aqueous extract of Houttuynia cordata and 1 mM $AgNO_3$ were combined in different volume ratios (1:5, 1:10, 2:5, 2:10, and 3:5 v/v) and stirred continuously at 1080 rpm for 3 hours at 50 °C. In a specific preparation, 20 mL of the leaf extract was mixed with 100 mL of 0.1 mM $AgNO_3$ solution and incubated in a shaker incubator at 300 rpm and 37 °C for 48 hours. Over time, the deep green solution gradually transitioned to a yellowish-brown hue, signifying the reduction of Ag^+ to Ag^0. The successful formation of Hc-AgNPs was confirmed by a dark brown color change. The nanoparticles were subsequently collected by centrifugation at 15,000 rpm for 25 minutes. To eliminate loosely bound molecules and impurities, the collected nanoparticles were thoroughly washed with ethanol and acetone. Finally, the purified Hc-AgNPs were obtained in powder form [23, 24].

Conjugation of Hc-AgNPs with Curcumin

A suspension of Hc-AgNPs (20 mg/mL in distilled water) was combined with 10 mg of thiol-polyethylene glycol-amine ($HS\text{-}PEG_2K\text{-}NH_2$) and subjected to sonication for 1 hour. The mixture was then allowed to stand at room temperature for 24 hours to enable surface coating and ligand exchange between Hc-AgNPs and PEG. Subsequently, curcumin (20 mg/mL) was dissolved in 20 mL of phosphate-buffered saline (PBS) containing 0.05 N sodium hydroxide and added to the PEGylated Hc-AgNPs (PEG–Hc-AgNPs) solution. The mixture was then sonicated for 20 minutes at room temperature without heat and incubated in the dark at 4 °C for 24 hours to facilitate curcumin binding. To purify the conjugate, three rounds of centrifugation were carried out at 18,000 rpm for 45 minutes, followed by resuspension of the pellet in sterile distilled water. This washing step was repeated three more times to remove any unbound molecules. Finally, the purified curcumin-conjugated nanoparticles (Cur–PEG–HcAgNPs) were stored at 4 °C for subsequent conjugation with folic acid [25, 26].

Preparation of Calibration Curve

The concentration of curcumin (CuR) was measured using a UV spectrophotometric method. A stock solution of 1 mg/mL was prepared by dissolving CuR in ethanol [27, 28]. This stock solution was then diluted with double-distilled water to obtain a final concentration of 10 µg/mL. Aliquots of these solutions were placed in a quartz cuvette and analyzed using a UV spectrophotometer (Perkin Elmer, USA) to determine the maximum absorbance wavelength (λmax) within the 200–800 nm range, with double-distilled water serving as the blank. A standard calibration curve was constructed by plotting absorbance against concentration for CuR solutions in the range of 1–10 µg/mL.

Surface Modification of Cur–PEG–HcAgNPs

The final step of the experiment involved functionalizing Cur–PEG–HcAgNPs with folic acid (FA). To achieve this, 10 mg of Cur–PEG–HcAgNPs

Journal of Chemical Health Risks

www.jchr.org

JCHR (2025) 15(2), 701-713 | ISSN:2251-6727

was dispersed in 20 mL of aqueous alkali and continuously stirred for 1 hour to facilitate effective surface modification. Following this, 200 µL of ethyl dimethylaminopropyl carbodiimide (EDC) and 200 µL of N-hydroxysuccinimide (NHS) were added dropwise to activate the nanoparticle surface for conjugation [29-31]. Subsequently, 5 mL of folic acid (FA) in an alkaline medium was introduced and mixed to ensure efficient binding. The reaction mixture was then centrifuged at 4000 rpm for 30 minutes to remove unbound and precipitated nanoparticles. The supernatant was lyophilized for 15–18 hours, and the final product was stored at 8°C for future applications. The bioactive compound profiles of H. cordata, Cur–PEG–HcAgNPs, and FA–Cur–PEG–HcAgNPs were quantitatively assessed using standard methods to determine total phenolic and flavonoid content. Additionally, the concentration of surface-bound folate on Cur–PEG–HcAgNPs was measured.

Drug Loading

The synthesized FA–Cur–PEG–HcAgNPs were first dissolved in 0.5 mL of ethanol and then diluted with an appropriate volume of distilled water. The resulting solution was filtered through a 0.45 µm membrane filter to remove any particulate impurities. The concentration of curcumin in the nanoparticles was then measured at 423 nm using a UV-Vis spectrophotometer. The curcumin loading capacity of the green silver nanoparticles was calculated using the following equation:

Drug loading capacity=Amount of Curcumin in FA-Cur-Hc-AgNPs/ Total amount of Curcumin used for loading X100

Determination of Drug Entrapment Efficiency (%DEE)

The encapsulation efficiency (%EE) of curcumin in FA–Cur–PEG–HcAgNPs was assessed by analyzing the supernatant obtained during nanoparticle synthesis [32,33]. After centrifugation at 6000 rpm for 15 minutes, the clear supernatant was carefully collected, and its absorbance was recorded at 423 nm using a UV-Vis spectrophotometer. The percentage of drug entrapment efficiency (%DEE) was then determined using the following equation:

$\%DEE$= (Amount of free curcumin present/Total theoretical amount used)×100

In Vitro Curcumin Release

The in vitro drug release study was performed using the dialysis bag method. Green-synthesized AgNPs, equivalent to 5 mg of curcumin, were placed inside a cellulose dialysis bag (molecular weight cutoff: 12,000 KDa) along with a small volume of phosphate-buffered saline (PBS) as the dissolution medium [34, 35]. The bag was securely sealed at both ends and submerged in a beaker containing 1× PBS at pH 6.4. At specific time intervals, 5 mL aliquots were withdrawn and immediately replaced with fresh dissolution medium to maintain sink conditions. This process was continued for up to 180 minutes. The amount of curcumin released was quantified using a UV-Vis spectrophotometer at 423 nm.

Characterization of FA-Cur–PEG–HcAgNPs

The physicochemical and morphological characteristics of Hc, Hc-AgNPs, and FA-Cur-Hc-AgNPs were analyzed using standard nano-characterization techniques [27-30]. The surface plasmon resonance of the nanoparticles was confirmed using a UV-Vis spectrophotometer. The polydispersity index, average particle size, and zeta potential of HcAgNPs and FA–Cur–Hc-AgNPs were measured using a Malvern Mastersizer 2000 instrument. To understand the molecular interactions between the plant material, $AgNO_3$, Hc-AgNPs, conjugated curcumin, folic acid, and FA-Cur-Hc-AgNPs, Fourier-transform infrared (FT-IR) spectroscopy (FT-IR PerkinElmer, USA) was employed. Size and shape are crucial characteristics of synthesized nanoparticles, as these properties play a significant role in drug delivery to cancer cells [36]]. The morphology and elemental composition of the nanoparticles were examined using a transmission electron microscope (TEM, JEM-2100F, Japan) and a scanning electron microscope (SEM, JEOL-JSM 1200EX, Japan).

***In-vitro* cytotoxicity study**

The study was outsourced to Mr. Biologist, CRO, Guwahati, Assam. MCF-7 cells were cultured in DMEM supplemented with 10% (v/v) fetal bovine serum under standard conditions (37°C, 5% CO_2). The culture medium was refreshed every 2–3 days. For the

Journal of Chemical Health Risks

www.jchr.org

JCHR (2025) 15(2), 701-713 | ISSN:2251-6727

experiment, cells were seeded in 96-well plates at a density of 2 × 10^4 cells per well in 200 µL of medium and incubated at 37°C in a 5% CO_2 atmosphere for 24 hours to allow cell attachment, forming approximately half-confluent monolayers [33-34]. After incubation, the culture medium was removed, and the cells were treated with nine different concentrations of the test sample. Untreated cells in the medium served as the control group. Plates were incubated under the same conditions for another 24 hours. Post-treatment, cell morphology and viability were observed under an inverted microscope. The medium was then replaced with 100 µL of fresh medium, followed by the addition of 10 µL of MTT reagent to each well. Plates were further incubated for 4 hours at 37°C in a 5% CO_2 atmosphere. After incubation, 100 µL of solubilization solution was added to each well, and the plates were left undisturbed for 1 hour. Once complete solubilization of formazan crystals was confirmed, absorbance was measured at 570 nm using a microplate reader.

IC_{50} values were determined by plotting a logarithmic graph of test sample concentrations against percentage cell survival. The percentage of cell survival was calculated using the formula:

Percent Cell Survival (%) = (Absorbance of Test/Absorbance of Control) ×100

To assess apoptotic changes induced by FA–Cur–HcAgNPs, the Acridine Orange-Ethidium Bromide (AO-EtBr) dual staining method was used. Cells were incubated with FA–Cur–HcAgNPs, and fluorescence analysis was performed using a fluorescence microscope. AO and EtBr dyes were used to distinguish between necrotic, apoptotic, and normal cells [35]. AO dye penetrates live cells with intact membranes, binding to DNA and emitting green fluorescence, indicating normal and healthy cells. In contrast, EtBr stains dead and late apoptotic cells, emitting orange-red fluorescence [37-38].

4. Results

Numerous studies have emphasized the potential of bioactive plant compounds and phytogenic metal nanoparticles (NPs) as promising alternatives and adjuncts in therapeutic applications. However, enhancing their pharmacological efficacy through nanotechnological modifications remains a key research focus. In this study, folic acid and starch were utilized as surface-functionalization agents to enhance the anticancer activity of Hc-AgNPs, which were biosynthesized using an aqueous extract of *Houttuynia cordata*.

Physicochemical Characterization of Folic Acid-Conjugated Curcumin-Loaded *Houttuynia cordata*-Mediated Silver Nanoparticles (FA–Cur–HcAgNPs)

In this study, Houttuynia cordata extract was utilized as a reducing and stabilizing agent for the green synthesis of folic acid- and curcumin-functionalized silver nanoparticles (FA–Cur–HcAgNPs) using silver nitrate ($AgNO_3$) as the metal precursor. Various extract-to-metal precursor ratios (1:4, 1:8, 2:4, 2:8, and 3:5) were explored to optimize nanoparticle synthesis, with formation initially confirmed by UV-visible spectroscopy. The synthesized nanoparticles exhibited a characteristic surface plasmon resonance (SPR) peak at 360 nm. A distinct color transition from green to dark brown further validated the reduction of Ag^+ ions and successful nanoparticle formation. Among the tested formulations, the 1:4 Hc–$AgNO_3$ ratio displayed the most prominent absorption peak at 350 nm, suggesting efficient nanoparticle synthesis. Following the conjugation of curcumin and folic acid, the absorption peak exhibited a slight blue shift to 340 nm, confirming the successful functionalization of the green-synthesized silver nanoparticles. This spectral shift further substantiated the effective incorporation of curcumin and folic acid into the HcAgNPs.

Particles size analysis and zeta potential

Zeta potential analysis plays a pivotal role in nanomaterials research by assessing particle size, size distribution, polydispersity index (PDI), and surface charge—key factors influencing nanoparticle stability and bioavailability. For optimal nanotherapeutic applications, an ideal particle size below 200 nm and a PDI under 0.2 are desirable to enhance systemic circulation, dispersion, and therapeutic efficiency. In this study, the size, zeta potential, and PDI of Houttuynia cordata-mediated silver nanoparticles (HcAgNPs) were meticulously evaluated before and after functionalization with aminated curcumin and folic acid **(Table 1).**

Journal of Chemical Health Risks

www.jchr.org

JCHR (2025) 15(2), 701-713 | ISSN:2251-6727

Table 1. Particle size, zeta potential and poly dispersity index of FA-Cur-Hc-AgNPs in different ratio of Hc-Cur-AgNPs and FA-Cur-Hc-AgNPs.

Reaction mixture	Conjug-ation. ratio (v/v)	Particle size (nm±SD)	Zeta potential (mV±SD)	PDI±SD
Hc-AgNPs (Hc: AgNO3)	1:4	158.2±1.12	-33.5±0.12	0.188±0.12
	1:8	224.5±1.05	-47.6±0.23	0.395±0.04
	2:4	278.3±0.76	-21.7±0.32	0.243±0.02
	2:8	385.2±0.22	-25.3±0.16	0.412±0.06
	3:5	486.6±0.54	-9.9±0.11	0.541±0.03
Cur-Hc-AgNPs (Cur:Hc-AgNPs)	9:1	184.2±0.07	-39.7±0.07	0.224±0.16
	8:2	137.4±1.14	-44.6±0.22	0.354±0.13
	7:3	294.5±1.02	-23.7±0.13	0.397±0.11
	6:4	416.3±0.54	-9.6±0.16	0.678±0.08
FA-Cur-Hc-AgNPs FA: Cur-Hc-AgNPs	2:8	176.2±1.53	-41.3±1.12	0.156±0.21

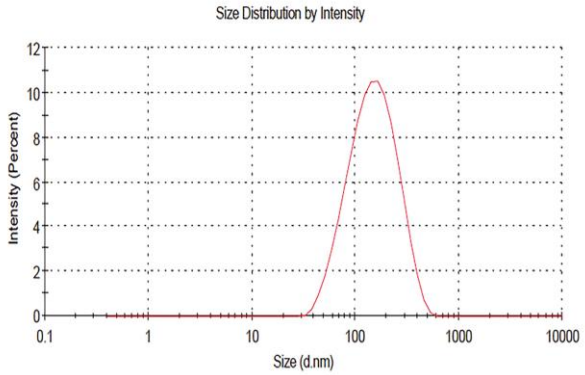

Figure 1a: Particle Size analysis of FA-Cur-Hc-AgNPs

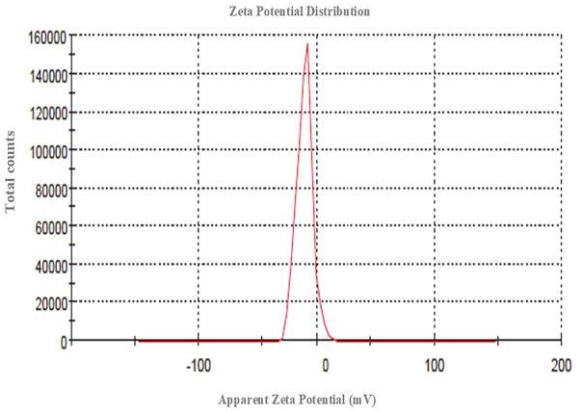

Figure 1b: Zeta potential analysis of FA-Cur-Hc-AgNPs

Hc-AgNPs were synthesized using varying extract-to-$AgNO_3$ ratios (1:4, 1:8, 2:4, 2:8, and 3:5), where higher silver nitrate concentrations led to an increase in particle size. The optimized 1:4 formulation exhibited an average particle size of 158.21 nm, a PDI of 0.188, and a zeta potential of –33.51 mV, ensuring colloidal stability. Upon conjugation with curcumin at a 9:1 ratio, the nanoparticles increased in size to 184.21 nm, with a PDI of 0.224 and a zeta potential of –39.72 mV (Figure 1a,b).

The structural integrity and surface charge distribution of FA–Cur–HcAgNPs were influenced by two key modifications: (i) amine-functionalized curcumin serving as a stabilizing and capping agent for the biosynthesized AgNPs and (ii) folic acid conjugation via EDC/NHS-mediated coupling, enabling amide bond formation between free amine groups. This functionalization significantly enhanced the

Journal of Chemical Health Risks

www.jchr.org

JCHR (2025) 15(2), 701-713 | ISSN:2251-6727

nanoparticle's positive surface charge, fostering strong electrostatic interactions with negatively charged cancer cell membranes. The resulting increase in cellular uptake underscores the potential of FA–Cur–HcAgNPs as a targeted drug delivery system, offering enhanced anticancer efficacy.

Drug loading and % drug entrapment efficiency

The prepared Cur-Hc-AgNPs demonstrated efficient drug loading, exceeding 72%. However, the main optimization parameters were reaction time, temperature, and the drug-to-Ag precursor ratio, which must be considered during drug loading capacity. The entrapment efficiency and drug loading of Cur-Hc-AgNPs ranged from 63.12±1.13% to 76.31±2.42% and from 91.11±2.03% to 94.12±3.02%, respectively. The prepared Cur-Hc-AgNPs exhibited efficient drug loading, surpassing 72%, indicating their potential as an effective nanocarrier system. However, the optimization of key formulation parameters—including reaction time, temperature, and the drug-to-Ag precursor ratio—is essential for achieving consistent and improved drug loading efficiency. The encapsulation efficiency (EE) and drug loading (DL) of Cur-Hc-AgNPs varied from 63.12±1.13% to 76.31±2.42% and from 91.11±2.03% to 94.12±3.02%, respectively, demonstrating a relatively high retention of the active compound within the nanoparticle matrix. These variations in EE and DL suggest that factors such as nanoparticle size, surface charge, and interaction between curcumin (Cur) and the hydrocolloid (Hc) matrix play crucial roles in encapsulation efficiency. The hydrophobic nature of curcumin, coupled with its affinity for silver nanoparticles, may enhance its loading within the nanosystem. However, further studies are required to elucidate the impact of different reaction conditions on the stability and release kinetics of the drug. Additionally, the high drug loading observed in Cur-Hc-AgNPs may contribute to prolonged drug release, reducing the frequency of dosing and improving therapeutic efficacy. Future research should focus on optimizing synthesis conditions, evaluating in vitro drug release profiles, and assessing biological interactions to establish Cur-Hc-AgNPs as a promising drug delivery platform.

FT-IR analysis

Fourier Transform Infrared (FT-IR) spectroscopy was employed to analyze the molecular interactions and functional groups present in Houttuynia cordata extract, biosynthesized HcAgNPs, curcumin, folic acid, and the final FA–Cur–HcAgNPs formulation within the spectral range of 4000–500 cm^{-1} (Figure 2). The FT-IR spectrum of H. cordata extract revealed distinct absorption bands corresponding to O–H stretching (hydroxyl and phenolic groups), N–H stretching (amine groups), C–H stretching (aliphatic and aromatic compounds), C=O stretching (carbonyl functional groups from flavonoids and ketones), C=C stretching (aromatic and flavonoid systems), and C–O stretching (phenols and carbohydrates). The $AgNO_3$ spectrum exhibited characteristic bands associated with N–O asymmetric and symmetric stretching (NO_3^- group) and O–Ag vibrations. Curcumin displayed absorption peaks characteristic of O–H stretching, C=O stretching (β-diketone and conjugated carbonyl moieties), C=C stretching (aromatic system), and C–O–C stretching (ether linkages). Similarly, folic acid exhibited well-defined bands corresponding to O–H stretching (carboxyl groups), N–H stretching (amide and amine groups), C=O stretching (carboxyl and amide functional groups), C=N stretching (pteridine ring system), and C–H bending (aromatic moieties).

The FT-IR spectrum of FA–Cur–HcAgNPs provided strong evidence of successful functionalization through significant spectral shifts and broadening of key absorption bands. The expansion of the O–H and N–H stretching vibrations in the range of 3400–3200 cm^{-1} indicated enhanced hydrogen bonding and molecular interactions with the AgNP surface. A notable shift in the C=O stretching peak from 1700 cm^{-1} to 1650 cm^{-1} confirmed the effective conjugation of curcumin and folic acid onto the nanoparticle surface. Additional peaks corresponding to C=N (pteridine ring), C=C (aromatic system), and C–O (phenolics, ether linkages, and carbohydrates) further substantiated the successful functionalization. Moreover, the emergence of new absorption bands in the range of 500–450 cm^{-1} suggested Ag–O and Ag–N interactions, corroborating nanoparticle formation and biomolecule binding. These spectral modifications collectively confirm the efficient synthesis, functionalization, and stabilization of FA–

Journal of Chemical Health Risks
www.jchr.org
JCHR (2025) 15(2), 701-713 | ISSN:2251-6727

Cur–HcAgNPs, reinforcing their potential for targeted drug delivery applications.

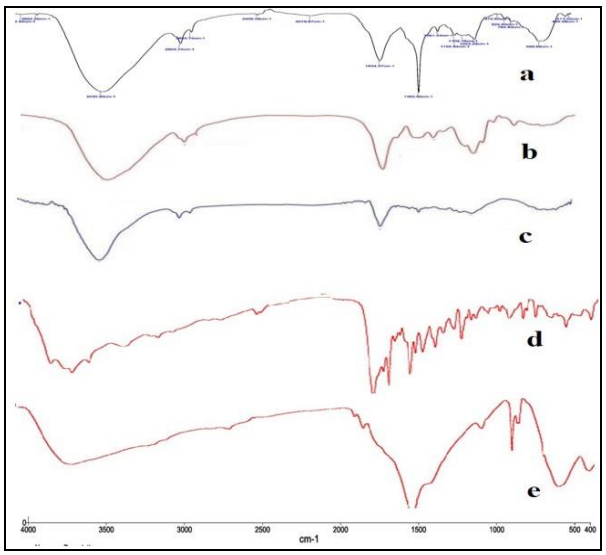

Figure 2. FT-IR spectra of (a) H. cordata plant extract, (b) Silver (c) Curcumin (d) Folic acid and (e) FA-Cur-Hc-AgNPs

TEM and SEM analysis

Transmission electron microscopy (TEM) and scanning electron microscopy (SEM) analyses were conducted to evaluate the morphological characteristics and size distribution of HcAgNPs and FA–Cur–HcAgNPs **(Figure 3).** The particle size of HcAgNPs varied across different synthesis ratios, ranging from 158.21 nm to 486.62 nm. In contrast, Cur–HcAgNPs demonstrated a reduced particle size, averaging 121.42 nm, with a broader distribution spanning 184.21 nm to 416.34 nm. SEM imaging revealed the formation of nanoparticles with distinct hexagonal and oval morphologies, displaying multiple structural layers. Notable nanoparticle agglomeration was observed, likely due to the presence of phytochemicals from Houttuynia cordata extract, which acted as both a reducing and stabilizing agent. Furthermore, the nanoformulation exhibited characteristic surface modifications, confirming the successful conjugation of curcumin and folic acid onto the AgNP framework. These structural insights highlight the effective synthesis and functionalization of FA–Cur–HcAgNPs, demonstrating their potential for biomedical applications.

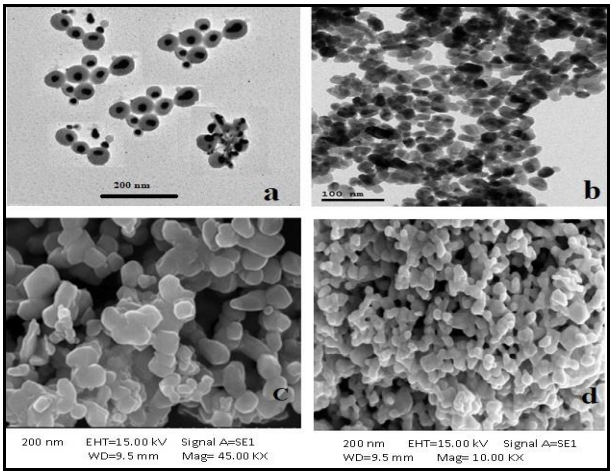

Figure 3. TEM (a,b) and SEM (c,d) images of FA-Cur-Hc-AgNPs

In-vitro drug release characteristics

The in vitro drug release study demonstrated a significantly higher release of curcumin (Cur) from silver nanoparticles at pH 5.5, which closely mimics the acidic environment of mature endosomes in cancer cells **(Figure 4).** The drug release exhibited a time-dependent increase across all pH conditions, with 73.32 ± 0.68% of nanoparticles releasing the drug after 72 hours at pH 5.5.

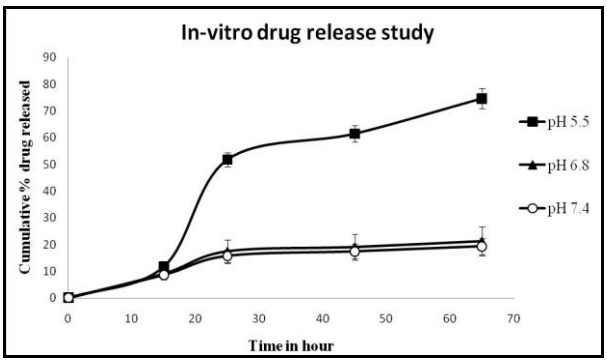

Figure 4. In-vitro drug release characteristics of curcumin loaded green silver nanoparticles in three different pH medium

In contrast, at pH 6.8 and pH 7.4, the release was significantly lower, measuring 22.24 ± 1.00% and 20.75 ± 0.11%, respectively. This trend highlights the pH-responsive nature of the nanoparticles, where drug release is enhanced in acidic conditions and reduced in neutral or slightly basic environments. Such a release

Journal of Chemical Health Risks

www.jchr.org

JCHR (2025) 15(2), 701-713 | ISSN:2251-6727

profile is advantageous for anticancer applications, as it ensures that the therapeutic agent is preferentially released in the tumor microenvironment, thereby improving drug efficacy while minimizing systemic toxicity.

Results of Cytotoxic and Apoptotic Effects of FA-Cur-Hc-AgNPs on MCF-7 Cells

The MTT assay demonstrated a pronounced cytotoxic effect of FA-Cur-Hc-AgNPs on MCF-7 breast cancer cells, with cell viability decreasing in a time-dependent manner **(Table 2).** At the initial time point (0 hours), all experimental groups exhibited a confluent monolayer, indicating uniform cell distribution before treatment. However, by 12 hours, a marked reduction in cell density was observed in the FA-Cur-Hc-AgNP-treated group, suggesting the early onset of apoptotic or cytotoxic responses. After 24 hours of incubation, significant cell death was evident, highlighting the enhanced therapeutic efficacy of FA-Cur-Hc-AgNPs. This effect is likely attributed to folic acid functionalization, which promotes selective uptake by folate receptor-overexpressing MCF-7 cells **(Figure 5).**

Table 2. Results of MTT assay and percentage of cell survival

Conc. (PPM)	Absorbance			Average	% Cell Survival			Average% cell Survival
Control (CTRL)	1.118	1.407	1.115	1.213	92.14	115.96	91.90	100.00
750	0.971	1.017	1.188	1.059	80.03	83.82	97.91	87.25
1500	1.307	1.143	1.056	1.169	107.72	94.20	87.03	96.32
3750	0.925	1.028	0.986	0.980	76.24	84.73	81.26	80.74
7500	0.47	0.306	0.67	0.482	38.74	25.22	55.22	39.73
15000	0.436	0.171	0.452	0.353	35.93	14.09	37.25	29.09
IC50 Value	5313.34							

Comparative analysis revealed that while Cur-Hc-AgNPs and Hc-AgNPs also exhibited cytotoxic effects, their potency was notably lower than that of FA-Cur–Hc-AgNPs. The control group, comprising blank nanoparticles, showed minimal cytotoxicity, confirming the primary role of curcumin and silver nanoparticles in mediating cell death. These results emphasize the potential of FA-Cur-Hc-AgNPs as an effective targeted nanotherapeutic for breast cancer treatment.

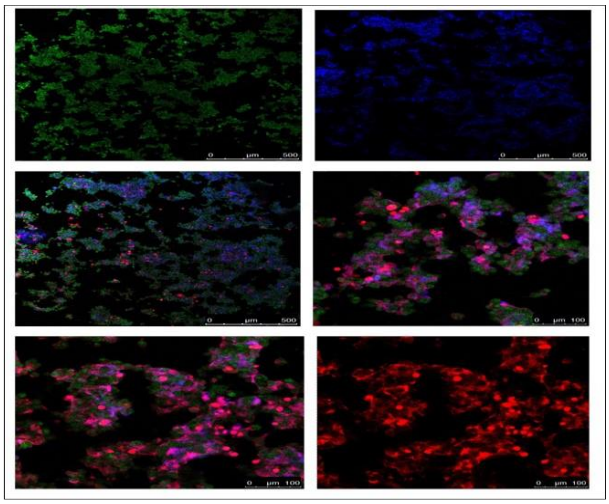

Figure 5. Cell apoptosis studies of FA-Cur-Hc-AgNPs on normal and cancer cells

Apoptotic Induction Assessed by AO/EtBr Staining

The apoptotic effects of FA–Cur–HcAgNPs were further validated through acridine orange/ethidium bromide (AO/EtBr) dual staining, which differentially marks viable, apoptotic, and necrotic cells. In fluorescence microscopy images, nuclear staining (blue) highlights DNA, while green fluorescence (AO) identifies viable and early apoptotic cells. In contrast, ethidium bromide selectively permeates late apoptotic and necrotic cells, producing red fluorescence. The composite fluorescence images (Figure 4) reveal a gradual transition from predominantly green fluorescence to increased red fluorescence, indicating progressive apoptosis. The nuclear stain (blue) further enables visualization of chromatin condensation and nuclear fragmentation—hallmarks of apoptosis. Over time, a notable increase in condensed or fragmented nuclei was observed, reinforcing the apoptotic nature of FA–Cur–HcAgNP-induced cytotoxicity. These findings collectively support the efficacy of FA–Cur–HcAgNPs in inducing apoptosis in MCF-7 cells, underscoring their potential as a targeted nanotherapeutic strategy for breast cancer treatment.

5. Discussion

The successful green synthesis and functionalization of folic acid-conjugated, curcumin-loaded *Houttuynia cordata*-mediated silver nanoparticles (FA–Cur–HcAgNPs) demonstrated their potential as an effective nanotherapeutic system. The study employed

Journal of Chemical Health Risks

www.jchr.org

JCHR (2025) 15(2), 701-713 | ISSN:2251-6727

Houttuynia cordata extract as a natural reducing and stabilizing agent, ensuring an eco-friendly and biocompatible synthesis process. The formation of FA–Cur–HcAgNPs was initially confirmed by UV-visible spectroscopy, where a distinct surface plasmon resonance (SPR) peak at 360 nm indicated the reduction of silver ions and nanoparticle formation. The subsequent conjugation with curcumin and folic acid led to a blue shift in the SPR peak, confirming successful functionalization. The color transition from green to dark brown further supported the nanoparticle synthesis.

Physicochemical characterization revealed an optimal particle size of ~158.21 nm, a polydispersity index (PDI) of 0.188, and a highly negative zeta potential (−33.51 mV), ensuring good colloidal stability. Upon functionalization with curcumin and folic acid, the particle size increased slightly (184.21 nm), with improved surface charge distribution, further enhancing nanoparticle stability. FT-IR spectral analysis confirmed key functional group interactions, indicating successful incorporation of curcumin and folic acid onto the nanoparticle surface. TEM and SEM imaging revealed uniform, hexagonal, and oval-shaped nanoparticles, confirming their structural integrity and stability.

A crucial aspect of this study was the evaluation of drug loading and encapsulation efficiency. FA–Cur–HcAgNPs exhibited high drug entrapment efficiency (63.12–76.31%) and drug loading capacity (91.11–94.12%), suggesting their effectiveness as a nanocarrier system. The pH-responsive drug release profile demonstrated significantly higher curcumin release (~73.32%) in an acidic environment (pH 5.5), mimicking the tumor microenvironment, while minimal release occurred at physiological pH (7.4). This controlled release mechanism is advantageous for targeted cancer therapy, reducing systemic toxicity and improving drug efficacy.

The cytotoxicity assessment via MTT assay confirmed a dose- and time-dependent reduction in MCF-7 breast cancer cell viability, with FA–Cur–HcAgNPs displaying superior anticancer activity compared to non-functionalized nanoparticles. The selective uptake of nanoparticles by folate receptor-overexpressing MCF-7 cells confirmed their targeting ability. Apoptotic induction, as observed through AO/EtBr dual staining, demonstrated chromatin condensation and nuclear fragmentation, highlighting their ability to trigger programmed cell death.

Overall, FA–Cur–HcAgNPs show great promise as a targeted nanotherapeutic for breast cancer treatment. Future studies should focus on in vivo validation, mechanistic insights into cellular uptake, and optimizing synthesis parameters to enhance clinical applicability.

6. Conclusion

The findings of this study highlight the successful green synthesis and functionalization of folic acid-conjugated curcumin-loaded silver nanoparticles (FA-Cur-HcAgNPs) using Houttuynia cordata extract as a reducing and stabilizing agent. The physicochemical characterization confirmed the effective formation of nanoparticles with a distinct surface plasmon resonance peak, optimal particle size, and stable zeta potential, ensuring their colloidal stability and bioavailability. The functionalization with curcumin and folic acid further enhanced their structural integrity and targeting ability, as evidenced by FT-IR spectral shifts and TEM/SEM morphological assessments. The in-vitro drug release study demonstrated a pH-responsive behavior, with a significantly higher release of curcumin at acidic pH (5.5), mimicking the tumor microenvironment. This controlled drug release pattern underscores the potential of FA-Cur-HcAgNPs in targeted cancer therapy, maximizing therapeutic efficacy while minimizing off-target effects. The cytotoxicity analysis against MCF-7 breast cancer cells through the MTT assay revealed a time-dependent reduction in cell viability, with FA-Cur-HcAgNPs displaying superior anticancer efficacy compared to non-functionalized nanoparticles. The selective uptake of these nanoparticles by folate receptor-overexpressing cancer cells highlights their potential as an effective nanocarrier system for breast cancer treatment. Additionally, AO/EtBr dual staining confirmed the induction of apoptosis, with progressive chromatin condensation and nuclear fragmentation over time. The strong apoptotic effect of FA-Cur-HcAgNPs indicates their capability to trigger programmed cell death in cancer cells, further supporting their role as a targeted nanotherapeutic strategy. In conclusion, the successful synthesis, functionalization, and in-vitro evaluation of FA-Cur-HcAgNPs demonstrate their

Journal of Chemical Health Risks

www.jchr.org

JCHR (2025) 15(2), 701-713 | ISSN:2251-6727

immense potential in nanomedicine. Their pH-sensitive drug release, targeted delivery, and cytotoxic effects establish them as a promising candidate for breast cancer therapy. Future studies should focus on in-vivo validation and detailed mechanistic insights to advance these nanoparticles toward clinical applications.

References

1. Visser, L. L.; Groen, E. J.; van Leeuwen, F. E.; Lips, E. H.; Schmidt, M. K.; Wesseling, J. Predictors of an Invasive Breast Cancer Recurrence after DCIS: A Systematic Review and Meta-Analyses. Cancer Epidemiol. Biomarkers Prev. 2019, 28 (5), 835–845. https://doi.org/10.1158/1055-9965.EPI-18-0976.
2. Mariotto, A. B.; Etzioni, R.; Hurlbert, M.; Penberthy, L.; Mayer, M. Estimation of the Number of Women Living with Metastatic Breast Cancer in the United States. Cancer Epidemiol. Biomarkers Prev. 2017, 26 (6), 809–815. https://doi.org/10.1158/1055-9965.EPI-16-0889.
3. Ghoncheh, M.; Pournamdar, Z.; Salehiniya, H. Incidence, Mortality, and Epidemiology of Breast Cancer in the World. Asian Pac. J. Cancer Prev. 2016, 17 (S3), 43–46. https://doi.org/10.7314/apjcp.2016.17.s3.43.
4. Britt, K. L.; Cuzick, J.; Phillips, K. A. Key Steps for Effective Breast Cancer Prevention. Nat. Rev. Cancer 2020, 11 (1), 1–20. https://doi.org/10.1038/s41568-020-0266-x.
5. Ganesan, K.; Wang, Y.; Gao, F.; Liu, Q.; Zhang, C.; Li, P.; et al. Targeting Engineered Nanoparticles for Breast Cancer Therapy. Pharmaceutics 2021, 13 (11), 1829. https://doi.org/10.3390/pharmaceutics13111829.
6. Malik, J. A.; Ansari, J. A.; Ahmed, S.; Khan, A.; Ahemad, N.; Anwar, S. Nano-Drug Delivery System: A Promising Approach against Breast Cancer. Ther. Deliv. 2023, 14 (6), 357–381. https://doi.org/10.4155/tde-2023-0020.
7. Sattari, R.; Khayati, G. R.; Hoshyar, R. Biosynthesis and Characterization of Silver Nanoparticles Capped by Biomolecules by Fumaria Parviflora Extract and Their Cytotoxicity against MDA-MB-468 Cell Lines. Mater. Chem. Phys. 2019, 241, 122438. https://doi.org/10.1016/j.matchemphys.2019.122438.
8. Saravanakumar, K.; Chelliah, R.; MubarakAli, D.; Oh, D. H.; Kathiresan, K.; Wang, M. H. Unveiling the Potentials of Biocompatible Silver Nanoparticles on Human Lung Carcinoma A549 Cells and Helicobacter pylori. Sci. Rep. 2019, 9 (1), 1–8. https://doi.org/10.1038/s41598-019-42112-1.
9. Ju, L.; Zhang, J.; Wang, F.; Zhu, D.; Pei, T.; He, Z.; et al. Chemical Profiling of Houttuynia cordata Thunb. by UPLC-Q-TOF-MS and Analysis of Its Antioxidant Activity in C2C12 Cells. J. Pharm. Biomed. Anal. 2021, 204, 114271.
10. Rathi, R.; Roy, S.; Misra, A.; Singh, S. K. Ethnobotanical Notes on Houttuynia cordata Thunb. in North-Eastern Region of India. Indian J. Nat. Prod. Resour. 2014, 4, 432–435.
11. Kumar, M.; Prasad, S. K.; Hemalatha, S. A Current Update on the Phytopharmacological Aspects of Houttuynia cordata Thunb. Pharmacogn. Rev. 2014, 8 (15), 22.
12. Khuraijam, J. Ethnobotanical Uses of Houttuynia cordata by Meitei Community of Manipur, India. Ethnobotany 2014, 26, 106–110.
13. Wu, Z.; Deng, X.; Hu, Q.; Xiao, X.; Jiang, J.; Ma, X.; Wu, M. Houttuynia cordata Thunb.: An Ethnopharmacological Review. Front. Pharmacol. 2021, 12, 714694.
14. Shingnaisui, K.; Dey, T.; Manna, P.; Kalita, J. Therapeutic Potentials of Houttuynia cordata Thunb. against Inflammation and Oxidative Stress: A Review. J. Ethnopharmacol. 2018, 220, 35–43.
15. Mariadoss, A. V. A.; Vinayagam, R.; Xu, B.; Venkatachalam, K.; Sankaran, V.; Vijayakumar, S.; et al. Phloretin-Loaded Chitosan Nanoparticles Enhance the Antioxidant and Apoptotic Mechanisms in DMBA-Induced Experimental Carcinogenesis. Chem.-Biol. Interact. 2019, 308, 11–19. https://doi.org/10.1016/j.cbi.2019.05.008.
16. Saravanan, A.; Senthil Kumar, P.; Karishma, S.; Vo, D. V. N.; Jeevanantham, S.; Yaashikaa, P. R.; et al. A Review on Biosynthesis of Metal Nanoparticles and Its Environmental Applications. Chemosphere

2021, 264 (Pt 2), 128580. https://doi.org/10.1016/j.chemosphere.2020.128580.

17. Pradhan, S.; Rituparna, S.; Dehury, H.; Dhall, M.; Singh, Y. D. Nutritional Profile and Pharmacological Aspect of Houttuynia cordata Thunb. and Their Therapeutic Applications. Pharmacol. Res. Mod. Chin. Med. 2023, 9, 100311. https://doi.org/10.1016/j.prmcm.2023.100311.
18. Sun, L.; Liu, H.; Ye, Y.; Lei, Y.; Islam, R.; Tan, S.; et al. Smart Nanoparticles for Cancer Therapy. Signal Transduct. Target Ther. 2023, 8 (418), 1–15. https://doi.org/10.1038/s41392-023-01642-x.
19. Gomes, H. I. O.; Martins, C. S. M.; Prior, J. A. V. Silver Nanoparticles as Carriers of Anticancer Drugs for Efficient Target Treatment of Cancer Cells. Nanomaterials 2021, 11 (4), 964. https://doi.org/10.3390/nano11040964.
20. Mariadoss, A. V. A.; Ramachandran, V.; Shalini, V.; Agilan, B.; Franklin, J. H.; Sanjay, K.; et al. Green Synthesis, Characterization, and Antibacterial Activity of Silver Nanoparticles by Malus domestica and Its Cytotoxic Effect on MCF-7 Cell Line. Microb. Pathog. 2019, 135, 103609.
21. Padil, V. V. T.; Cernik, M. Green Synthesis of Copper Oxide Nanoparticles Using Gum Karaya as a Biotemplate and Their Antibacterial Application. Int. J. Nanomed. 2013, 8, 889. https://doi.org/10.2147/IJN.S40599.
22. Mukherjee, P. K. Extraction and Other Downstream Procedures for Evaluation of Herbal Drugs. In Quality Control and Evaluation of Herbal Drugs; Elsevier, 2019; pp. 195–236.
23. Cheng, W.; Nie, J.; Xu, L.; Liang, C.; Peng, Y.; Liu, G.; et al. pH-Sensitive Delivery Vehicle Based on Folic Acid-Conjugated Polydopamine-Modified Mesoporous Silica Nanoparticles for Targeted Cancer Therapy. ACS Appl. Mater. Interfaces 2017, 9 (23), 18462–18473. https://doi.org/10.1021/acsami.7b02457.
24. Thulasidasan, A. K. T.; Retnakumari, A. P.; Shankar, M.; Vijayakurup, V.; Anwar, S.; Thankachan, S.; et al. Folic Acid Conjugation Improves the Bioavailability and Chemosensitizing Efficacy of Curcumin-Encapsulated PLGA-PEG Nanoparticles Towards Paclitaxel Chemotherapy. Oncotarget 2017, 8 (64), 107374–107389. https://doi.org/10.18632/oncotarget.22376.
25. Parker, N.; Turk, M. J.; Westrick, E. W.; Lewis, J. D.; Low, P. S.; Leamon, C. P. Folate Receptor Expression in Carcinomas and Normal Tissues Determined by a Quantitative Radioligand Binding Assay. Anal. Biochem. 2005, 338 (2), 284–293. https://doi.org/10.1016/j.ab.2004.12.026.
26. Mansoori, G. A.; Brandenburg, K. S.; Shakeri-Zadeh, A. A Comparative Study of Two Folate-Conjugated Gold Nanoparticles for Cancer Nanotechnology Applications. Cancers 2010, 2 (4), 1911–1928. https://doi.org/10.3390/cancers2041911.
27. Leone, J. P.; Bhargava, R.; Theisen, B. K.; Hamilton, R. L.; Lee, A. V.; Brufsky, A. M. Expression of High-Affinity Folate Receptor in Breast Cancer Brain Metastasis. Oncotarget 2015, 6 (30), 30327–30333. https://doi.org/10.18632/oncotarget.4639.
28. Nawaz, F. Z.; Kipreos, E. T. Emerging Roles for Folate Receptor FOLR1 in Signaling and Cancer. Trends Endocrinol. Metab. 2022, 33 (3), 159–174. https://doi.org/10.1016/j.tem.2021.12.003.
29. Zhang, Z.; Wang, J.; Tacha, D. E.; Li, P.; Bremer, R. E.; Chen, H.; et al. Folate Receptor α Associated with Triple-Negative Breast Cancer and Poor Prognosis. Arch. Pathol. Lab. Med. 2014, 138 (7), 890–895. https://doi.org/10.5858/arpa.2013-0309-OA.
30. Sathiyaseelan, K.; Saravanakumar, K.; Mariadoss, A. V. A.; Wang, M. H. Biocompatible Fungal Chitosan Encapsulated Phytogenic Silver Nanoparticles Enhanced Antidiabetic, Antioxidant, and Antibacterial Activity. Int. J. Biol. Macromol. 2020, 153, 63–71. https://doi.org/10.1016/j.ijbiomac.2020.02.291.
31. Butzbach, K.; Konhäuser, M.; Fach, M.; Bamberger, D. N.; Breitenbach, B.; Epe, B.; et al. Receptor-Mediated Uptake of Folic Acid-Functionalized Dextran Nanoparticles for Applications in Photodynamic Therapy. Polymers (Basel) 2019, 11 (5), 896. https://doi.org/10.3390/polym11050896.

32. Hasan, S. S.; Singh, S.; Parikh, R. Y.; Dharne, M. S.; Patole, M. S.; Prasad, B.; et al. Bacterial Synthesis of Copper/Copper Oxide Nanoparticles. J. Nanosci. Nanotechnol. 2008, 8 (6), 3191–3196. https://doi.org/10.1166/jnn.2008.095.

33. Danaei, M.; Dehghankhold, M.; Ataei, S.; Hasanzadeh Davarani, F.; Javanmard, R.; Dokhani, A.; et al. Impact of Particle Size and Polydispersity Index on the Clinical Applications of Lipidic Nanocarrier Systems. Pharmaceutics 2018, 10 (2), 57. https://doi.org/10.3390/pharmaceutics10020057.

34. Stati, G.; Rossi, F.; Trakoolwilaiwan, T.; Tung, L. D.; Mourdikoudis, S.; Thanh, N. T. K.; et al. Development and Characterization of Curcumin-Silver Nanoparticles as a Promising Formulation to Test on Human Pterygium-Derived Keratinocytes. Molecules 2022, 27 (1), 282. https://doi.org/10.3390/molecules27010282.

35. Dutta, D.; Pajaniradje, S.; Nair, A. S.; Chandramohan, S.; Bhat, S. A.; Manikandan, E.; et al. An In Vitro Study of Active Targeting and Anti-Cancer Effect of Folic Acid-Conjugated Chitosan-Encapsulated Indole Curcumin Analogue Nanoparticles. Int. J. Biol. Macromol. 2024, 282 (Pt 5), 136990. https://doi.org/10.1016/j.ijbiomac.2024.136990.

36. Liu, J. L.; Pan, Y. Y.; Chen, O.; Luan, Y.; Xue, X.; Zhao, J. J.; et al. Curcumin Inhibits MCF-7 Cells by Modulating the NF-κB Signaling Pathway. Oncol. Lett. 2017, 14 (5), 5581–5584. https://doi.org/10.3892/ol.2017.6860.

37. Saharkhiz, S.; Zarepour, A.; Zarrab, A. Empowering Cancer Therapy: Comparing PEGylated and Non-PEGylated Niosomes Loaded with Curcumin and Doxorubicin on MCF-7 Cell Line. Bioengineering (Basel) 2023, 10 (10), 1159. https://doi.org/10.3390/bioengineering10101159.

38. Raphael, R.; Aswathy, W. F.; Anila, E. I. In Vitro Cytotoxicity Studies of Ga_2O_3 Microstructures on L929 and MCF-7 Cell Lines Using MTT Assay. MRS Commun. 2024, 14 (6), 1359–1363. https://doi.org/10.1557/s43579-024-00647-z.

Acknowledgement

We sincerely extend our heartfelt gratitude to the Contract Research Organization, Mr. Biologist, Guwahati for facilitating the outsourcing of the MTT assay and cell apoptosis studies.

Data availability

All authors have made significant contributions to the conception, design, data acquisition, analysis, and interpretation of the study. Any data required from the research work can be accessed by sending mail request to the corresponding authors.

FUNDING

The authors affirm that this research was conducted without any external funding or financial support.

Competing interests

The authors declare that there are no financial or any other potential conflicts of interest associated with this work.

E**thical approvals**

This research does not involve any experiments conducted on animals or human participants.